

**Evaluation of Carbon Nanotube Thin Films for Optically
Transparent Microwave Applications Using On-Wafer
Probing of Corbino Disc Test Structures**

**by Ryan C. Toonen, Julia B. Doggett, S. Gary Hirsch, Mathew P. Ivill,
Eric H. Ngo, Clifford W. Hubbard, Henning Richter, and Ramesh Sivarajan**

ARL-TR-6362

March 2013

NOTICES

Disclaimers

The findings in this report are not to be construed as an official Department of the Army position unless so designated by other authorized documents.

Citation of manufacturer's or trade names does not constitute an official endorsement or approval of the use thereof.

Destroy this report when it is no longer needed. Do not return it to the originator.

Army Research Laboratory

Aberdeen Proving Ground, MD 21005-5069

ARL-TR-6362

March 2013

Evaluation of Carbon Nanotube Thin Films for Optically Transparent Microwave Applications Using On-Wafer Probing of Corbino Disc Test Structures

**Ryan C. Toonen, S. Gary Hirsch, Mathew P. Ivill,
Eric H. Ngo, and Clifford W. Hubbard
Weapons and Materials Research Directorate, ARL**

**Julia B. Doggett
George Washington University**

**Henning Richter and Ramesh Sivarajan
Nano-C, Inc.**

REPORT DOCUMENTATION PAGE			Form Approved OMB No. 0704-0188		
Public reporting burden for this collection of information is estimated to average 1 hour per response, including the time for reviewing instructions, searching existing data sources, gathering and maintaining the data needed, and completing and reviewing the collection information. Send comments regarding this burden estimate or any other aspect of this collection of information, including suggestions for reducing the burden, to Department of Defense, Washington Headquarters Services, Directorate for Information Operations and Reports (0704-0188), 1215 Jefferson Davis Highway, Suite 1204, Arlington, VA 22202-4302. Respondents should be aware that notwithstanding any other provision of law, no person shall be subject to any penalty for failing to comply with a collection of information if it does not display a currently valid OMB control number. PLEASE DO NOT RETURN YOUR FORM TO THE ABOVE ADDRESS.					
1. REPORT DATE (DD-MM-YYYY) March 2013		2. REPORT TYPE Final		3. DATES COVERED (From - To) November 2012	
4. TITLE AND SUBTITLE Evaluation of Carbon Nanotube Thin Films for Optically Transparent Microwave Applications Using On-Wafer Probing of Corbino Disc Test Structures			5a. CONTRACT NUMBER		
			5b. GRANT NUMBER		
			5c. PROGRAM ELEMENT NUMBER		
6. AUTHOR(S) Ryan C. Toonen, Julia B. Doggett, [*] S. Gary Hirsch, Mathew P. Ivill, Eric H. Ngo, Clifford W. Hubbard, Henning Richter, [†] and Ramesh Sivarajan [†]			5d. PROJECT NUMBER		
			5e. TASK NUMBER		
			5f. WORK UNIT NUMBER		
7. PERFORMING ORGANIZATION NAME(S) AND ADDRESS(ES) U.S. Army Research Laboratory ATTN: RDRL-WMM-E Aberdeen Proving Ground, MD 21005-5069			8. PERFORMING ORGANIZATION REPORT NUMBER ARL-TR-6362		
9. SPONSORING/MONITORING AGENCY NAME(S) AND ADDRESS(ES)			10. SPONSOR/MONITOR'S ACRONYM(S)		
			11. SPONSOR/MONITOR'S REPORT NUMBER(S)		
12. DISTRIBUTION/AVAILABILITY STATEMENT Approved for public release; distribution is unlimited.					
13. SUPPLEMENTARY NOTES [*] Science and Engineering Apprenticeship Program, George Washington University/Department of Defense, Washington, D.C., 20052 [†] Nano-C, Inc., 33 Southwest Park, Westwood, MA 02090					
14. ABSTRACT We present a generalized technique, involving the on-wafer probing of Corbino disc test structures, for conveniently evaluating conducting films of arbitrary thickness in terms of complex conductivity and related physical parameters. Using this method, we have electrically characterized partially transparent carbon nanotube thin films at DC and microwave frequencies (including the L-, S- and C-bands). Test structures with disc diameters ranging from ~50 μm to 500 μm and disc-to-concentric-ring gaps ranging from ~30 μm to 150 μm were investigated at temperatures ranging from (295.85 ± 0.62) K to (396.75 ± 0.72) K. Additionally, we characterized the thin film in terms of its room temperature optical transmission, at wavelengths ranging from 200 to 2500 nm, in order to evaluate this material as an optically transparent microwave conductor.					
15. SUBJECT TERMS transparent conductors, carbon nanotubes, corbino disc, microwave spectroscopy					
16. SECURITY CLASSIFICATION OF:			17. LIMITATION OF ABSTRACT	18. NUMBER OF PAGES	19a. NAME OF RESPONSIBLE PERSON
a. REPORT	b. ABSTRACT	c. THIS PAGE			Ryan C. Toonen
Unclassified	Unclassified	Unclassified	UU	28	19b. TELEPHONE NUMBER (Include area code) 410-306-4536

Contents

List of Figures	iv
List of Tables	v
1. Introduction	1
2. Methods	2
2.1 Fabrication of Corbino Discs	2
2.2 Lumped Element Circuit Models of Corbino disc Test Structures	2
2.3 Measurements from Corbino Disc Test Structures	7
3. Results and Discussion	10
3.1 Electrical Characterizations.....	10
3.2 Optical Characterizations	12
4. Conclusions	14
5. References	16
List of Symbols, Abbreviations, and Acronyms	18
Distribution List	19

List of Figures

Figure 1. Flow of processes used for fabricating Corbino disc test structures. (a) CNT thin film deposition. (b) probe pad fabrication.	2
Figure 2. (a) <i>Bird's-eye-view</i> of a Corbino disc test structure (shown not to scale). (b) Photograph of actual Corbino disc test structures fabricated on a CNT-coated, sapphire substrate. (c) Three-dimensional representation of a Corbino disc test structure (shown not to scale). (d) SEM micrograph of a cross-section of the MUT.....	3
Figure 3. (a) Transmission line and its equivalent distributed-element circuit model. (b) Equivalent schematic models of a generalized Corbino disc test structure.	5
Figure 4. Probing configuration of a Corbino disc test structure.....	8
Figure 5. Apparatus for temperature controlled characterizations of (a) current vs. voltage, (b) DC resistance, and (c) microwave complex conductivity.....	8
Figure 6. (a) Trace of measured current vs. sourced voltage obtained from an electrometer. (b) Measured values of sheet resistance vs. disc-to-ring gap for different values disc diameter obtained from a multimeter.....	11
Figure 7. (a) Real and (b) imaginary parts of complex conductivity; (c) γh ; and (d) $\sigma' \sigma \epsilon''^2$ vs. frequency for different values of substrate temperature.....	11
Figure 8. (a) Low-frequency sheet resistance RS , LF , AC surface resistance RS , and (b) skin depth as a function of substrate temperature for test signal frequencies of $f = 1, 4.5$ and 8 GHz.	12
Figure 9. Optical transmission vs. wavelength for a CNT film on sapphire substrate and a solitary CNT film. The range of human visibility is highlighted in yellow.	13

List of Tables

Table 1. Admittance model of the Corbino disc for special case scenarios.	6
Table 2. FoMs for electrical and optical performance of a solitary CNT thin film.	14

INTENTIONALLY LEFT BLANK.

1. Introduction

There is currently a strong military interest in the use of optically transparent conducting films for microwave and millimeter-wave applications. The electrical properties of a number of Transparent Conducting Films (TCFs), in addition to Carbon Nanotube (CNT) networks, have been evaluated for DC and low frequency applications. Such films have been composed of materials that include: Transparent Conducting Oxides (TCOs) (1), Intrinsically Conducting Polymers (ICPs) (2), and other nano-structured materials (for example exfoliated graphene (3) and elemental metal ultrathin films (4) and nano-wire grids (5). Surprisingly, relatively few TCFs have been evaluated for use in microwave and/or millimeter-wave electronics. Several research groups have investigated the use of TCOs such as Indium Tin Oxide (ITO) and Fluorine-doped Tin Oxide (FTO) for fabricating transparent microwave antennas (6). Additionally, transparent CNT films have been characterized at microwave frequencies in terms of their electromagnetic shielding properties (7, 8). However, all of these studies indicate that there are significant limitations associated with physically realizing useable transparent high-frequency conductors; the main difficulty is the inherent tradeoff between optical transparency and electrical conduction.

In this report, we present our findings from an investigation on the DC and microwave conduction and optical transmission properties of partially transparent thin films composed of CNT networks. From these films, we have fabricated Corbino disc test structures for the purpose of on-wafer probe testing. Historically, Corbino discs have been used to study vortex phenomena associated with magnetoresistance (the Corbino effect) (9); however, in this study, we have used such structures to characterize the temperature dependent DC sheet resistance and AC complex conductivity, over the L-, S-, and C-bands (1 to 8 GHz), without applying an extrinsic magnetic field. It should be noted that the microwave Corbino reflection technique has previously been used to characterize CNT thin films as well as metallic and superconducting materials (7). All of these efforts relied on pressing a sample of the Material Under Test (MUT) against an open end of a coaxial cable. The novelty of our measurement scheme is the aspect of on-wafer probing. This technique has given us the freedom to rapidly evaluate Corbino disc test structures of different sizes, disc-to-spacing ratios, and MUT thicknesses.

2. Methods

2.1 Fabrication of Corbino Discs

Our Corbino discs were prepared by first depositing a blanket layer of CNTs over a 2-in diameter, c-axis sapphire wafer, using a method first described by Wu, et al. (10), and then fabricating highly conductive, thick film, probe pads over this CNT-coated substrate. As depicted in figure 1a, a sacrificial, CNT-infused polycarbonate membrane was first swathed over the sapphire. This wafer was then placed in a solvent bath that dissolved away the polymer matrix and left behind a CNT film. As shown in figure 1b, the transparent CNT film was then coated with two different types of photoresists: MicroChem LOR 30B, based on Poly(methyl glutarimide) (PMGI), and Microposit SC-1827, a common imaging resist whose main ingredient is Propylene Glycol Monomethyl Ether Acetate (PGMEA). A metal stack consisting of a 50 nm chrome adhesion layer, a 2.5 μm copper thick film, and a 50 nm gold capping layer was then e-beam evaporated over the photoresist bilayer. Following this step, the masked portion of the metal was then lifted off using the method suggested by the MicroChem Corporation (11). The process lifting off sharp-profile metal thick films was aided by the use of a photoresist bilayer with a self-aligned undercut. Finally, the resulting test structures were cleaned in a heated acetone bath (kept at 55 $^{\circ}\text{C}$), rinsed with isopropanol, and dried with nitrogen gas. Optical microscope inspection did not reveal evidence of photoresist residue left on the CNT thin films.

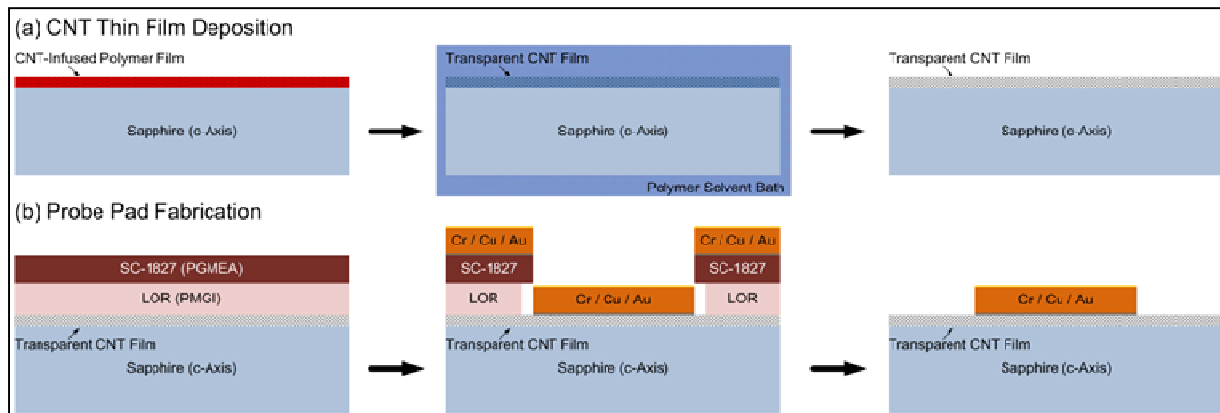


Figure 1. Flow of processes used for fabricating Corbino disc test structures. (a) CNT thin film deposition. (b) probe pad fabrication.

2.2 Lumped Element Circuit Models of Corbino disc Test Structures

The cartoon of figure 2a illustrates the geometry and field distribution of a Corbino disc, which is a highly conductive disc of diameter d connected to a highly conductive concentric ring by a less conductive CNT network of radial length g . In this picture, we have assumed that a signal with a right-handed, Transverse Electro-Magnetic (TEM) mode propagates toward the CNT film. The symbols \vec{E} and \vec{H} represent the electric and magnetic fields, respectively. Figure 2b is a

photograph of actual test structures. In this array, the values of d included (50, 100, 150, 300, and 500) μm while the values g included (30, 45, 90, and 150) μm . Figure 2c depicts a not-to-scale, side view of the structures shown in figure 2a and b. Figure 2d is a Scanning Electron Microscope (SEM) micrograph of a cross-section view of the CNT thin film. From this picture we estimate the thickness as $h = (435 \pm 20)$ nm.

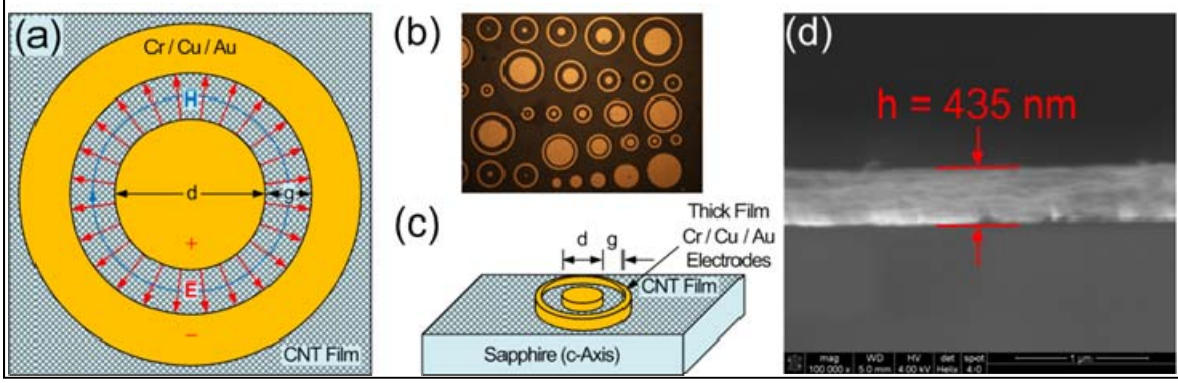


Figure 2. (a) *Bird's-eye-view* of a Corbino disc test structure (shown not to scale). (b) Photograph of actual Corbino disc test structures fabricated on a CNT-coated, sapphire substrate. (c) Three-dimensional representation of a Corbino disc test structure (shown not to scale). (d) SEM micrograph of a cross-section of the MUT.

An effective lumped-element circuit model can be used to represent the complex admittance Y (and impedance $Z = Y^{-1}$) of a Corbino disc fabricated over a thin film of arbitrary conductivity σ , permittivity ϵ , and permeability μ . In this picture, the Cr/Cu/Au probe pads are intended to be thought of as the coaxial signal conductor and its concentric ground shield while the CNT film acts as the medium of Electro-Magnetic (EM) propagation. To calculate the general expression for Y , we first assume that the film can be modeled as a coaxial transmission line of length h (the thickness of the film). This approximation is valid under the condition $h \ll g$. A transmission line, as schematically represented in figure 3a, can be modeled as a distributed-element circuit. In this picture, the z -axis defines the source-to-load position along the one dimensional transmission line. Conversely, the z' -axis provides a load-to-source frame of reference. In the limit $\Delta z \rightarrow 0$, the values R'_S and L'_S represent serially connected resistance-per-unit length and inductance-per-unit length while G'_p and C'_p represent values of shunted conductance-per-unit length and capacitance-per-unit length. In most cases, where the film thickness is significantly smaller than the disc gap ($h \ll g$), R'_S can be neglected. However, for the sake of completeness, we have included a general expression for R'_S (12) in terms of skin depth δ_S . A quasi-static expression for L'_S can be derived by application of Ampere's Law in integral form ($\oint_C \vec{H} \cdot d\vec{\ell} = I$), the constitutive relation $\vec{B} = \mu\vec{H}$, the surface integral $\Phi = \iint_S \vec{B} \cdot d\vec{s}$, and the circuital law of self-inductance ($L = \Phi/I$). Similarly, G'_p and C'_p can be calculated by application of Gauss' law in integral form ($\oint_S \vec{D} \cdot d\vec{s} = Q$), Ohm's field law ($\vec{J} = \sigma\vec{E}$), the constitutive relation $\vec{D} = \epsilon\vec{E}$,

the surface integral $I = \iint_S \vec{J} \cdot d\vec{s}$, Ohm's circuital law ($G = I V$), and the circuital law of capacitance ($C = Q V$). The solutions for these distributed elements are

$$R'_S = \frac{2}{\pi \sigma \delta_S} \left(\frac{d+g}{d(d+2g)} \right) \approx 0, \quad (1)$$

$$L'_S = \frac{\mu}{2\pi} \ln \left[\frac{d+2g}{d} \right] + \frac{R'_S}{\omega} \approx \frac{\mu}{2\pi} \ln \left[\frac{d+2g}{d} \right], \quad (2)$$

$$G'_P = 2\pi \sigma / \ln \left[\frac{d+2g}{d} \right], \quad (3)$$

and

$$C'_P = 2\pi \epsilon / \ln \left[\frac{d+2g}{d} \right]. \quad (4)$$

From equations 1–4, the waveguide's propagation impedance can be calculated from $Z_{WG} = \sqrt{(R'_S + j\omega L'_S)/(G'_P + j\omega C'_P)}$ (13):

$$Z_{WG} = \frac{\eta_c}{2\pi} \ln \left[\frac{d+2g}{d} \right] \quad (5)$$

where ω is the angular frequency of a monochromatic EM wave and η_c is the characteristic impedance of the film, which is given by

$$\eta_c = \sqrt{\frac{j\mu\omega}{\sigma + j\epsilon\omega}}. \quad (6)$$

The input impedance of the Corbino disc test structure, schematically represented by figure 3b, can be calculated using the general expression for load transformations

$$Z[z'] = Z_{WG} \frac{Z_L \cosh[\gamma z'] + Z_{WG} \sinh[\gamma z']}{Z_L \sinh[\gamma z'] + Z_{WG} \cosh[\gamma z']} \quad (13):$$

$$Z_{IN} = \lim_{Z_L \rightarrow \infty} \{Z[h]\} = Z_{WG} \coth[\gamma h]. \quad (7)$$

Finally, the lumped element model of figure 3b can be determined by equating a complex quantity $Y = G + jB$ (with a real and imaginary parts, the conductance and susceptance) to the input admittance $Y_{IN} = Z_{IN}^{-1}$. The resulting generalized relation is

$$G + jB = \frac{2\pi \tanh[\gamma h]}{\eta_c \ln \left[\frac{d+2g}{d} \right]}. \quad (8)$$

In equations 7 and 8, γ is the complex propagation constant given by $\gamma = \sqrt{j\mu\omega(\sigma + j\epsilon\omega)}$. At microwave frequencies, there exists some degree of ambiguity with respect to the physical meaning of the parameters of power dissipation (σ) and dispersion (ϵ and μ). For example, the effective finite conductance need not solely depend on physical mechanisms that impede the transport of charge carriers in a material but can also represent the influence of any mechanism that consumes energy (including microwave heating of a dielectric). Conversely, the effective parameters of permittivity and permeability can include the influence of conduction mechanisms that contribute to the storage of energy. For this reason, it is convenient (in a noncommittal

sense) to model the physical properties of a conducting material in terms of complex conductivity. To do so, we simply apply the substitutions: $\sigma \rightarrow \sigma'$ and $\epsilon\omega \rightarrow \sigma''_e$ to our previous expressions. Equation 6 can then be rewritten as $\eta_c = \sqrt{j\mu\omega/(\sigma' + j\sigma''_e)}$, and the complex propagation constant can then be rewritten as $\gamma = \sqrt{j\mu\omega(\sigma' + j\sigma''_e)}$. For mathematical convenience, γ can be separated into real and imaginary parts, $\gamma = \alpha + j\beta$, where α is the attenuation constant given by

$$\alpha = \sqrt{\mu\omega\sigma''_e} \left\{ \frac{1}{2} \left[\sqrt{1 + \left(\frac{\sigma'}{\sigma''_e}\right)^2} - 1 \right] \right\}^{1/2} \quad (9)$$

and β is the phase constant given by

$$\beta = \sqrt{\mu\omega\sigma''_e} \left\{ \frac{1}{2} \left[\sqrt{1 + \left(\frac{\sigma'}{\sigma''_e}\right)^2} + 1 \right] \right\}^{1/2}. \quad (10)$$

By definition, the quantity known as skin depth is simply the inverse of the attenuation constant ($\delta_s \equiv 1/\alpha$). Similarly, the wavelength of the EM wave propagating through the film can be defined in terms of β ($\lambda \equiv 2\pi/\beta$).

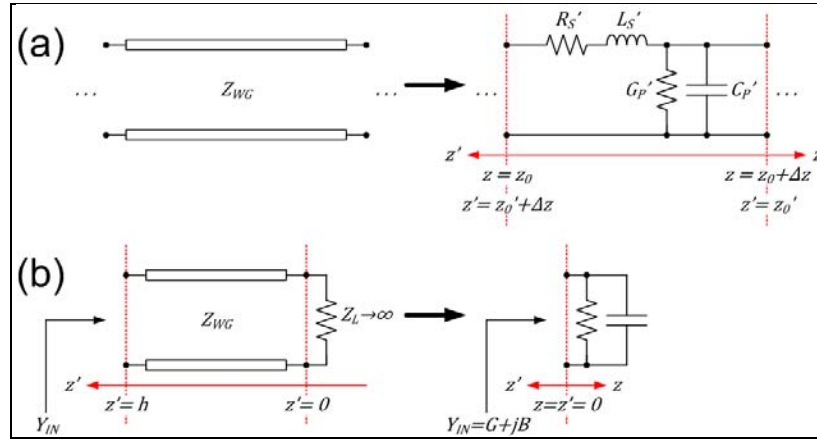


Figure 3. (a) Transmission line and its equivalent distributed-element circuit model. (b) Equivalent schematic models of a generalized Corbino disc test structure.

There are several special-case scenarios for which the generalized relation of equation 8 can be simplified. With regard to film thickness, there are two conditions that we will consider: the low-frequency case, which can be used when the film thickness is relatively small compared to the skin depth and wavelength of the EM wave ($|\gamma|h \ll 1$); and the case of generalized frequency, which is most appropriate to use when the film thickness is comparable to the skin depth and wavelength of the EM wave ($|\gamma|h \sim 1$). It does not make sense to consider the high frequency case, for which $|\gamma|h \gg 1$, as it is not appropriate to use a lumped element circuit to model in this scenario. In such a case, the film should be regarded as a bulk material and modeled by distributed impedances, as shown in figure 3a. With regard to material properties,

there are three conditions to consider that include: the case of a *poor* conductor, which is relevant when $(\sigma'/\sigma''_{\epsilon})^2 \ll 1$; the case of a generalized conductor, which is relevant when $(\sigma/\omega\epsilon)^2 \sim 1$; and the case of a *good* conductor, which is relevant when $(\sigma'/\sigma''_{\epsilon})^2 \gg 1$. The quantity $\sigma'/\sigma''_{\epsilon}$ is often referred to as the dielectric loss tangent ($\tan \delta_{\epsilon}$) and is commonly used as a Figure-of-Merit (FoM) for quantifying the conducting or insulating properties of a material. From the set of the five mentioned conditions, there are six permutations that each represents a special case scenario. For each of these scenarios, we have listed scaled expressions for G and B in table 1. It should be noted that when deriving the most general solutions (for a generalized conductor of generalized thickness), we have assumed that the quantity $\sigma'/\sigma''_{\epsilon}$ is both real and greater than or equal to zero in order to justify the substitution $\arg[\eta_C] = \frac{1}{2} \tan^{-1}[\sigma'/\sigma''_{\epsilon}]$. Although this substitution can usually be taken for granted, there are physical situations for which it does not hold. For instance, σ''_{ϵ} can be negative when an EM wave propagates through a material with a frequency that is greater than the plasma frequency of that medium (14).

Table 1. Admittance model of the Corbino disc for special case scenarios.

		Poor Conductor $(\sigma'/\sigma''_{\epsilon})^2 \ll 1$, $\alpha \approx (\sigma'/2)\sqrt{\mu\omega/\sigma''_{\epsilon}}$, $\beta \approx \sqrt{\mu\omega\sigma''_{\epsilon}}$	Generalized Conductor $(\sigma'/\sigma''_{\epsilon})^2 \sim 1$	Good Conductor $(\sigma'/\sigma''_{\epsilon})^2 \gg 1$, $\delta_s \approx \sqrt{2/\mu\omega\sigma'}$
Low Frequency $ \gamma h \ll 1$	$\frac{G}{2\pi} \ln \left[\frac{d+2g}{d} \right] =$	0	$\sigma' h$	$\sigma' h$
	$\frac{B}{2\pi} \ln \left[\frac{d+2g}{d} \right] =$	$\sigma''_{\epsilon} h$	$\sigma''_{\epsilon} h$	0
Generalized Frequency $ \gamma h \sim 1$	$\frac{G}{2\pi} \ln \left[\frac{d+2g}{d} \right] =$	$\frac{\sqrt{\sigma''_{\epsilon}} \sinh[2ah]}{\mu\omega \cos[2\beta h] + \cosh[2ah]}$	$\left(\frac{(\sigma')^2 + (\sigma''_{\epsilon})^2}{(\mu\omega)^2} \right)^{1/4} \frac{\sin \left[\frac{1}{2} \tan^{-1} \left[\frac{\sigma'}{\sigma''_{\epsilon}} \right] \right] \sin[2\beta h] + \cos \left[\frac{1}{2} \tan^{-1} \left[\frac{\sigma'}{\sigma''_{\epsilon}} \right] \right] \sinh[2ah]}{\cos[2\beta h] + \cosh[2ah]}$	$\frac{\sqrt{\sigma'} \sin \left[\frac{2h}{\delta_s} \right] + \sinh \left[\frac{2h}{\delta_s} \right]}{\sqrt{2\mu\omega} \cos \left[\frac{2h}{\delta_s} \right] + \cosh \left[\frac{2h}{\delta_s} \right]}$
	$\frac{B}{2\pi} \ln \left[\frac{d+2g}{d} \right] =$	$\frac{\sqrt{\sigma''_{\epsilon}} \sin[2\beta h]}{\mu\omega \cos[2\beta h] + \cosh[2ah]}$	$\left(\frac{(\sigma')^2 + (\sigma''_{\epsilon})^2}{(\mu\omega)^2} \right)^{1/4} \frac{\cos \left[\frac{1}{2} \tan^{-1} \left[\frac{\sigma'}{\sigma''_{\epsilon}} \right] \right] \sin[2\beta h] - \sin \left[\frac{1}{2} \tan^{-1} \left[\frac{\sigma'}{\sigma''_{\epsilon}} \right] \right] \sinh[2ah]}{\cos[2\beta h] + \cosh[2ah]}$	$\frac{\sqrt{\sigma'} \sin \left[\frac{2h}{\delta_s} \right] - \sinh \left[\frac{2h}{\delta_s} \right]}{\sqrt{2\mu\omega} \cos \left[\frac{2h}{\delta_s} \right] + \cosh \left[\frac{2h}{\delta_s} \right]}$

When performing a single port reflection measurement, with the aid of a network analyzer, two pieces of information are directly measured, the real and imaginary parts of the S_{11} scattering parameter. Therefore, only two material parameters can be extracted from such a measurement. The method of this measurement will be discussed in greater detail in the following subsection. In the low frequency cases, the two material parameters that can be determined include σ' and σ''_{ϵ} , provided h is known. If h is unknown, the film can be characterized in terms of $\tan \delta_{\epsilon} \approx G/B$ and its effective sheet resistance:

$$R_{S,LF} = \frac{1}{\sigma' h} = \left(\frac{G}{2\pi} \ln \left[\frac{d+2g}{d} \right] \right)^{-1}. \quad (11)$$

This parameter, given in units of Ω/Sq , is often used by integrated circuit engineers when designing with resistive layers of a set thickness (as specified by a foundry). Because the values of d and g would have been chosen by the engineer, they are assumed to be known with a high

level of accuracy; however, the film thickness h can be considerably more difficult to determine especially when the film is composed of a network of haphazardly meshed nanotubes.

In the most general case (the case of a generalized conductor for a generalized frequency), σ' and either σ''_ϵ or μ can be determined (using a numerical algorithm) provided that h and either μ or σ''_ϵ are known, respectively. However, in cases where the good conductor approximation can be assumed, it might not be possible to extract a value for σ''_ϵ . Similarly, if the low frequency approximation can be assumed, then it will be virtually impossible to extract a value for μ .

It is sometimes convenient to express microwave conductor loss in terms of AC surface resistance:

$$R_S = \frac{1}{\sigma' \delta_S}. \quad (12)$$

In the low frequency limit, δ_S will be considerably greater than h ; so, the distribution of current density throughout the conductor will be relatively constant, thereby yielding $R_S \approx R_{S,LF}$.

For all the cases listed in table 1, it should be possible to characterize the MUT in terms of its complex propagation constant γ . In principle, γ can be directly calculated for a given frequency using the extracted and assumed material parameters (σ' , σ''_ϵ and μ), as indicated by equations 8 and 9. However in real, linear materials, these parameters arise from frequency dependent micro-structural, molecular and atomic dispersion and loss mechanisms. So, σ' , σ''_ϵ and μ will also exhibit frequency dependence. Furthermore, for nonlinear materials these parameters will include harmonic and intermodulation distortion terms. Therefore, one should be careful when predicting the EM wave propagation characteristics of a material at one frequency based on material parameters extracted at another.

2.3 Measurements from Corbino Disc Test Structures

Figure 4 shows the probing configuration used in both our DC and microwave experiments. The abbreviations are signal (SIG), ground (GND), and guard (GRD). The substrate temperature was controlled using an ERS Electronic GmbH AirCool* SP72/300 temperature controller and a model TA1SA300H thermal wafer chuck that was mounted on a Cascade Microtech Summit 9000 Analytical Probe Station. For each temperature set point used in our experiments, an Omega Engineering, Inc., model HH-21A High Accuracy Digital Thermometer with a model 88001K type K surface probe directly recorded the surface temperature of the sapphire substrate.

* AirCool is a registered trademark of Cascade Microtech, Inc.

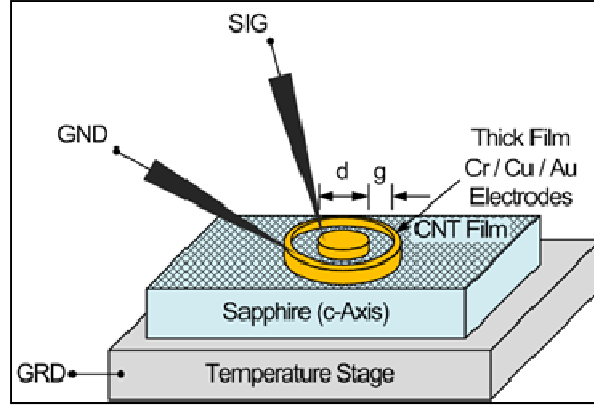


Figure 4. Probing configuration of a Corbino disc test structure.

In our experiments, we used two different methods for determining the low-frequency sheet resistance $R_{S,LF}$ at DC. The first method (shown in figure 5a) is known as a guarded $I-V$ characterization (15); we used a Keithley model 6517B Electrometer to perform these measurements. A voltage V_S was sourced to the SIG node of the DUT while current I_M was measured from its GND node; the conductance G of the Device Under Test (DUT) was extracted by simply determining the slope of the $I-V$ trace, and equation 10 was used to calculate $R_{S,LF}$. Both the temperature stage and the inner shield of the triaxial cable were kept at the GRD potential, which was kept at the GND potential by a buffered feedback network in the current meter, in order to eliminate substrate and cable leakage current from the measurement. This method is preferable for measuring DUTs whose resistance is significantly greater than that of the cabling and probe-to-sample contacts.

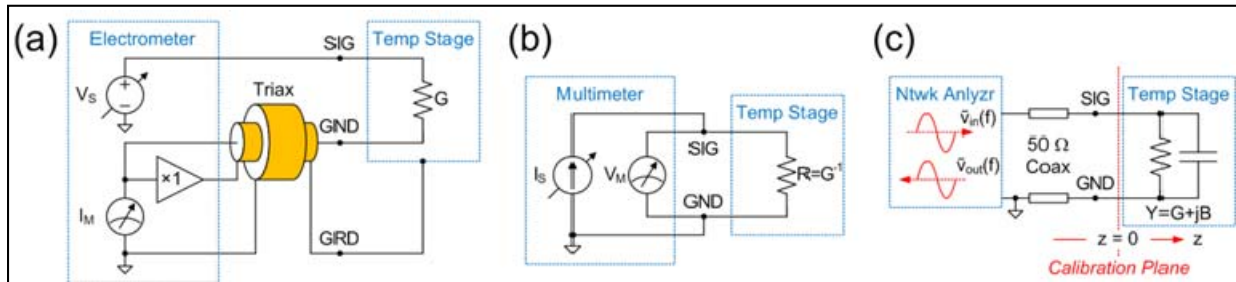


Figure 5. Apparatus for temperature controlled characterizations of (a) current vs. voltage, (b) DC resistance, and (c) microwave complex conductivity.

The second method of determining DC sheet resistance involved a four-wire $V-I$ characterizing (15) (as depicted in figure 5b). To perform this technique, we used the four-wire measurement mode of a Hewlett-Packard 34401A Digital Multimeter. We also used Cascade Microtech model DCP 150R Microprobes,* which allowed for the current and voltage wires to be internally connected near the probe-to-sample contacts (SIG and GND). This multimeter sourced a current I_S through the test structure, measured the resulting voltage V_M drop, and calculated the DUT resistance ($R = V_M/I_S$). Equation 10 was then applied with the extracted conductance $G = R^{-1}$ to determine $R_{S,LF}$. The four-wire measurement technique eliminates cable resistance from the resistance measurement. For this reason, it is preferable to use this technique when the DUT's resistance is comparable to that of the cabling. It is possible to also eliminate probe-to-sample contact resistance from this measurement by either using four separate single-tip probes or by using two dual-tip Kelvin probes (such as the Cascade Microtech model DCP 150K Microprobes).* However, for our test structures, the thick film probe pads allowed for negligible probe-to-sample contact resistance. In cases where probe-pad-to-film contact resistance is a concern, a four-point test structure such as a van der Pauw cloverleaf (15, 16) should be employed.

To extract material parameters at microwave frequencies from a Corbino disc DUT, we have measured scattering parameter data with an Agilent E8364B PNA Network Analyzer (as illustrated in figure 5c). The DUT was contacted using a GGB Industries model 50A-GS-150-P† high performance MW probe. The fictitious reference plane (defined at $z = 0$) which separates the apparatus from the DUT was established using a set of Short-Open-Load (SOL) standards from a GGB Industries CS-8 calibration substrate. In general, input impedance is readily obtainable from the complex S_{11} reflection parameter using the expression (13)

$$Z_{IN} = R_0 \left(\frac{1+S_{11}}{1-S_{11}} \right) \quad (13)$$

where R_0 is the intrinsic of the transmission line connected to the DUT; in our case, $R_0 = 50 \Omega$. In the previous subsection, we modeled the electrical characteristics of a Corbino disc as an admittance network ($Y_{IN} = Z_{IN}^{-1}$). From equation 12, the effective conductance G and susceptance B can be formulated, in terms of the real and imaginary parts of the S_{11} parameter, as

$$G = -\frac{1}{R_0} \left(1 - \frac{2 \operatorname{Re}[S_{11}]}{(1+\operatorname{Re}[S_{11}])^2 + (\operatorname{Im}[S_{11}])^2} \right) \quad (14)$$

and

$$B = -\frac{1}{R_0} \left(\frac{2 \operatorname{Im}[S_{11}]}{(1+\operatorname{Re}[S_{11}])^2 + (\operatorname{Im}[S_{11}])^2} \right), \quad (15)$$

* Microprobes is a registered trademark of Cascade Microtech, Inc.

† Model A-GA-150-P is a registered trademark of GGB Industries, Inc.

respectively. As expected, equations 13 and 14 are related to each other by Kramers–Kronig relationship. The relations from table 1 can be used to extract the material parameters (σ' and σ_ϵ'' or μ) as well as the complex propagation constant γ (by using equations 8 and 9) and the AC surface resistance R_S (from equation 11).

3. Results and Discussion

3.1 Electrical Characterizations

Figure 6a and b show data obtained by the two DC methods of measuring low frequency sheet resistance $R_{S,LF}$ as illustrated in figure 5a and b, respectively. The $I-V$ trace of figure 6a was obtained from a Corbino disc test structure with a disc diameter of $d = 300 \mu\text{m}$ and a disc-to-ring gap of $g = 45 \mu\text{m}$. The sample temperature was held fixed at $T = (298.85 \pm 0.62) \text{ K}$ during the measurement. Although the $I-V$ trace is highly linear, the extracted value of $R_{S,LF}$ exhibits a small amount of hysteresis. Sweeping the sourced voltage V_S in the upward direction yielded $R_{S,LF} = (1048.9 \pm 0.7) \Omega/\text{Sq}$ while sweeping V_S in the downward direction yielded $R_{S,LF} = (1055.7 \pm 0.6) \Omega/\text{Sq}$. The relatively small difference between these two extracted values could be entirely due to self-heating of the MUT. However, the error bar of $R_{S,LF}$ represents precision (calculated from the curve-fit) and not accuracy (determined by the instrumentation specifications); so, it is also possible that the $R_{S,LF}$ difference has resulted from instrumentation drift or a combination of this effect and self-heating of the MUT.

Figure 6b features $R_{S,LF}$ data obtained at room temperature ($T = (298.85 \pm 0.62) \text{ K}$) from Corbino disc test structures with disc diameters ranging from $\sim 50 \mu\text{m}$ to $500 \mu\text{m}$ and disc-to-concentric-ring gaps ranging from $\sim 30 \mu\text{m}$ to $150 \mu\text{m}$. Using the measurement technique illustrated in figure 5b, the low frequency sheet resistance value from the disc characterized in figure 6a, with dimensions of $d = 300 \mu\text{m}$ and $g = 45 \mu\text{m}$, was found to be $R_{S,LF} = (912.71 \pm 0.099) \Omega/\text{Sq}$. In this case, the error bar represents both the precision and accuracy of the measurement. Although the technique used to obtain this measurement automatically eliminates any influence of cable resistance, both measurements techniques include a non-zero contribution of contact resistance resulting from the probe-to-pad interface. It is likely that a contribution to the $R_{S,LF}$ measurement discrepancy (of roughly 14%) of two techniques is due to the probe-to-pad contact resistance. Regardless, there seems to be a trend present in the $R_{S,LF}$ data when plotted as a function of disc-to-ring gap g . As g is increased, the measured values of $R_{S,LF}$ obtained from test structures of different diameters, seem to converge. This trend suggests that there might be another parasitic resistance associated with the pad-to-MUT interface. Since the measured resistance of the test structure is directly proportional to g , the influence of the pad-to-MUT contact resistance becomes less significant as g is increased.

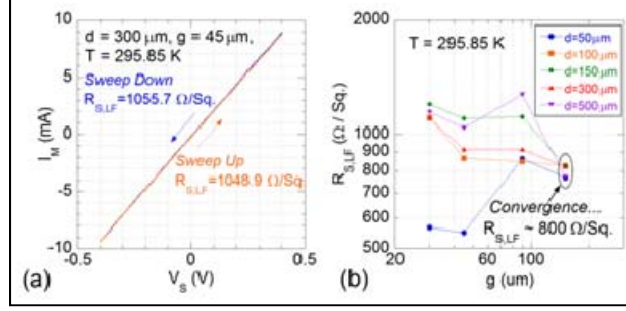


Figure 6. (a) Trace of measured current vs. sourced voltage obtained from an electrometer. (b) Measured values of sheet resistance vs. disc-to-ring gap for different values disc diameter obtained from a multimeter.

Figures 7a and b, respectively, show the frequency-dependent, real (σ') and imaginary parts (σ'') of the complex permittivity of the CNT thin film held at different substrate temperatures, $T = (295.85 \pm 0.62, 314.35 \pm 0.64, 348.25 \pm 0.68, 367.65 \pm 0.69, \text{ and } 396.75 \pm 0.72)$ K. For convenience, we have used cyclic frequency ($f = \omega/2\pi$), rather than angular frequency ω , as the independent variable of these graphs. The frequency range investigated included the L-band (1 to 2 GHz), the S-band (2 to 4 GHz), and the C-band (4 to 8 GHz). The parameters σ' and σ'' both exhibit a decreasing trend as a function of temperature. These individual traces were extracted using both the low frequency approximations and the generalized frequency expressions for the case of a generalized conductor. Both cases yielded the same numerical results, which is expected when $|\gamma|h \ll 1$. Figure 7c shows the frequency-dependent values of $|\gamma|h$ for different substrate temperatures. These curves indicate that even at the highest frequency (8 GHz), the low-frequency approximation ($|\gamma|h \ll 1$) still holds. Figure 7d displays the square of the extracted dielectric loss tangent $(\sigma'/\sigma'')^2$ as a function of frequency and temperature. The trends of these curves indicate that the merit of the CNT thin film as a conductor decreases as a function of increasing frequency. The value of $(\sigma'/\sigma'')^2$ features a peculiarity in its temperature dependence. At frequencies near $f = 1$ GHz, this FoM is directly proportional to temperature; however, in the neighborhood of $f \approx 3$ GHz, there is an onset of trend reversal that becomes more pronounced at higher frequencies. We currently do not have an explanation for this observed peculiarity.

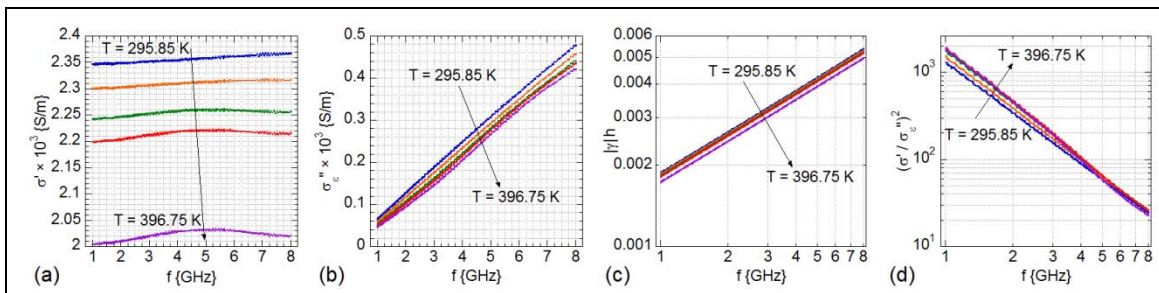


Figure 7. (a) Real and (b) imaginary parts of complex conductivity; (c) $|\gamma|h$; and (d) $(\sigma'/\sigma'')^2$ vs. frequency for different values of substrate temperature.

In figure 8a, we have plotted the DC and low frequency sheet resistances $R_{S,LF}$ and the AC surface resistance R_S as a function of substrate temperature for test signal frequencies of $f = (1, 4.5 \text{ and } 8) \text{ GHz}$. The DC value of $R_{S,LF}$ was obtained using the $I-V$ trace illustrated in figure 6a. The value of $R_{S,LF}$ indicates the effective resistance per square for the MUT of thickness h . The value of R_S represents the resistance per square that could be attained if the MUT were sufficiently thick, so that the low-frequency approximation ($|\gamma|h \ll 1$) would not apply. For *good* conductors, the condition of *sufficiently thick* usually implies that the MUT has a thickness of at least five skin depths (17). The temperature dependence of skin depth δ_S , calculated from the effective extracted parameters σ' and σ'' , is shown in figure 8b for test signal frequencies of $f = (1, 4.5 \text{ and } 8) \text{ GHz}$. Even at the highest frequency (8 GHz), the minimum value of δ_S was greater than $125 \mu\text{m}$, which is orders of magnitude times greater than the MUT thickness, $h = (435 \pm 20) \text{ nm}$. As implied by figure 7c, the low frequency approximation ($|\gamma|h \ll 1$) holds in all of the measured scenarios.

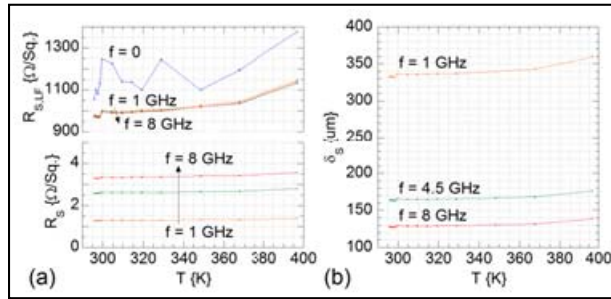


Figure 8. (a) Low-frequency sheet resistance $R_{S,LF}$, AC surface resistance R_S , and (b) skin depth as a function of substrate temperature for test signal frequencies of $f = (1, 4.5 \text{ and } 8) \text{ GHz}$.

3.2 Optical Characterizations

Optical characterization of the MUT was performed using a PerkinElmer, Inc., Lambda 950 UV/Vis Spectrophotometer.* As shown in figure 9, optical transmission \mathcal{T} data sets were collected with respect to two different spectral baselines. First, the spectrophotometer was calibrated with respect to air; measurement with respect to this baseline allowed us to characterize the optical transmission properties of the CNT film deposited on the sapphire substrate. A second measurement was performed after calibrating the spectrophotometer with respect to a bare sapphire substrate. This measurement allowed us to characterize the transmission properties of the solitary CNT film (without the influence of its substrate). Because the characterization was performed using a normal angle of incidence, no optical reflection \mathcal{R} data sets were collected.

*UV/Vis Spectrophotometer, is a registered trademark of PerkinElmer, Inc.

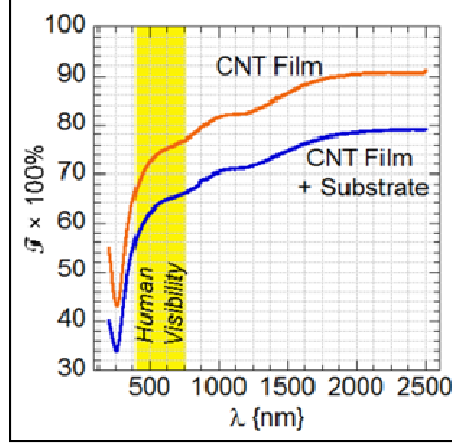


Figure 9. Optical transmission vs. wavelength for a CNT film on sapphire substrate and a solitary CNT film. The range of human visibility is highlighted in yellow.

In order to quantify the transmission characteristics in terms of a single FoM, we computed the weighted average \mathcal{T}_{ave} using the expression

$$\mathcal{T}_{ave} = \frac{\int_{\lambda_i}^{\lambda_f} \mathcal{T} \cdot d\lambda}{\lambda_f - \lambda_i}. \quad (16)$$

The integral in the numerator of equation 15 was calculated using a common numerical algorithm with an interpolation order of 3. For values of λ ranging over the full measured spectrum, (200 to 2500) nm, the value of \mathcal{T}_{ave} for the CNT film / substrate combination was found to be $\mathcal{T}_{ave} = 0.7042$ while that of the CNT film, by itself, was found to be $\mathcal{T}_{ave} = 0.8172$. Similarly, the average transmission values calculated over the range of human visibility, (390 to 750) nm, for the CNT film / substrate combination and solitary CNT film were found to be $\mathcal{T}_{ave} = 0.6302$ and $\mathcal{T}_{ave} = 0.7345$, respectively.

A FoM for evaluating the tradeoff between electrical conductivity σ' and optical absorption a has been used by Gordon (18). This quantity can be calculated from the low frequency sheet resistance $R_{S,LF}$ and the measured optical transmission \mathcal{T} and reflection \mathcal{R} :

$$\frac{\sigma'}{a} = \frac{-1}{R_{S,LF} \ln[\mathcal{T} + \mathcal{R}]} \quad (17)$$

In table 2, we have listed values of σ'/a corresponding to $\mathcal{T}_{ave} = 0.7345$, the optical transmission of a solitary CNT film averaged over the range of human visibility, and room temperature values of $R_{S,LF}$ measured at frequencies of $f = (0, 1, 4.5 \text{ and } 8)$ GHz. Since no optical reflection data sets were collected, we have evaluated σ'/a for the case of $\mathcal{R} = 0$. Under this condition, our FoM actually represents a lower bound value, $(\sigma'/a)_{low}$, where $\sigma'/a \geq (\sigma'/a)_{low}$. It is apparent from table 2 that the performance CNT thin film actually increases as

a function of microwave frequency. This quality is due to the fact that the skin depth and wavelength of the EM test signal become smaller, in reference to the film thickness h , with increasing frequency. This trend was quantified in the $|\gamma|h$ plot of figure 7c.

Table 2. FoMs for electrical and optical performance of a solitary CNT thin film.

f {GHz}	$R_{S,LF}$ { $\Omega/Sq.$ }	$(\sigma'/a)_{low} \times 10^{-3}$ { Ω^{-1} }
0	1055.6	3.070
1	979.72	3.308
4.5	976.07	3.320
8	971.50	3.336

4. Conclusions

Corbino disc test structures were fabricated for the purpose of measuring both the DC sheet resistance and microwave surface resistance of conducting CNT thin films. Additionally, we devised a convenient on-wafer probing technique for extracting physical parameters from conducting films of arbitrary thickness. We then used this microwave characterization technique to obtain effective values of complex conductivity from CNT films that were found to be electromagnetically thin with respect to the skin depth and wavelength of the EM test signals that were used to probe the MUT for physical information. The test signal frequencies ranged from (1 to 8) GHz (the L-, S-, and C-bands). We believe that we could improve the accuracy of future measurements and extend their frequency range as high as 50 GHz by employing a set of customized SOL calibration standards.

The DC sheet resistance measurements revealed a non-linear dependence on the disc-to-ring gap. This size dependence indicates that for small Corbino disc dimensions, the influence of the test structure on the extracted physical parameter values is non-negligible. It is possible that this phenomenon is related to the film stress imparted by the Corbino disc test structure on the CNT thin film.

The microwave characterizations of the CNT thin film revealed that the real part of the complex conductivity of ranges between $(2 \text{ and } 2.4) \times 10^3$ S/m, which is comparable to that of amorphous carbon that typically ranges between $(1.25 \text{ and } 2) \times 10^3$ S/m (19). From the DC and optical characterizations, we found the lower-bound value of a transparent conductor FoM to be $(\sigma'/a)_{low} = 3.070 \times 10^{-3} \Omega^{-1}$. This value is relatively low compared to those reported from common TCOs; for example, fluorine-doped zinc oxide (ZnO:F) can yield a value as high as $\sigma'/a = 7 \Omega^{-1}$ (18). So, the material we have evaluated is not an excellent optically transparent conductor, but there are still additional materials processing steps that could be used to improve its overall performance. The thin films used in our study were composed of

unseparated CNTs, which naturally occur with 2/3 being semiconducting and only 1/3 being conducting (20). Although filtering processes increase the overall production cost of the material, much research has been done to minimize this expense (21). Additionally, it is possible to increase the CNT thin film conductivity by using different methods of doping (22). However, any method used to increase conductivity will inevitably decrease the overall optical transparency. In the work of Wu, et al. (10), a de-doping technique was applied to increase conductivity, and it resulted in the shift of the maxima and minima of the optical transmission spectrum. In some parts of the spectrum, the local transmission increased whereas in other parts, the local transmission decreased. Although it might be the case that this type of band-structure engineering could be useful for optimizing transmission characteristics in certain applications, it is important to recognize that the overall optical transparency decreased as a fundamental consequence of increasing the electrical conductivity. Thus, engineering optically transparent microwave conductors is really a problem of compromise; where *compromise* can be optimized by maximizing the σ'/a FoM.

As a *cautionary tale*, we leave the reader with one final warning. Usually, an adequate microwave transmission line can be fabricated from a conductor with a thickness of just five skin depths (17). However, this simplified idea only applies to special cases involving *good* conductors (such as silver, gold and copper) that have relatively low permeability values. There is a common misconception (stemming from a misuse of this rule of thumb) that a *good* microwave transmission line can be realized from a high permeability, thin film by virtue of the fact that the skin depth would be relatively small. One must recognize that the parameter that should be minimized is actually the microwave surface resistance R_S , as expressed in equation 11. For example, a sufficiently thick silver strip (with $\sigma = 62.9 \times 10^6$ S/m, a relative permittivity of $\epsilon_r = 1$, and a relative permeability of $\mu_r = 1$) would yield $R_S = 7.92 \times 10^{-3}$ $\Omega/\text{Sq.}$; whereas, a sufficiently thick iron strip (with $\sigma = 10.4 \times 10^6$ S/m, $\epsilon_r = 1$, and $\mu_r = 5000$) would yield $R_S = 1.38$ $\Omega/\text{Sq.}$, which is 174 times more resistive!

This report reflects a portion of the results produced from a 3-year collaborative effort involving industry (Nano-C, Inc.), government (U.S. Army Research Laboratory [ARL]), and academic (Strano Research Group at the Massachusetts Institute of Technology) partners. Funding for these efforts was provided by the Institute for Soldier Nanotechnologies and the Department of Defense Science and Engineering Apprenticeship Program.

5. References

1. Ginley, D. S.; Hosono, H.; Paine, D. C. *Handbook of Transparent Conductors* (Springer Science+Business Media, New York, NY, 2010).
2. Seshadri, V.; Sotzing, G. A. Progress in Optically Transparent Conducting Polymers in *Organic Photovoltaics. Mechanisms, Materials, and Devices*; N. S. Sariciftci and S. S. Sun Ed., CRC Press, New York, NY, 2005.
3. Wassei, J. K.; Kaner, R. B. Graphene, a Promising Transparent Conductor. *Mater. Today* **2010**, *13*, 52–59.
4. O'Connor, B.; Haughn, C.; An, K. H.; Pipe, K. P.; Shtein, M. Transparent and Conductive Electrodes Based on Unpatterned, Thin Metal Films. *Appl. Phys. Lett.* **2008**, *93*, 223304.
5. Hu, L. B.; Wu, H.; Cui, Y. Metal Nanogrids, Nanowires, and Nanofibers for Transparent Electrodes. *MRS Bull* **2011**, *36*, 760–765.
6. Guan, N.; Furuya, H.; Delaume, D.; Ito, K. Antennas Made of Transparent Conductive Films. *PIERS Online* **2008**, *4*, 116–120.
7. Xu, H.; Anlage, S. M.; Hu, L.; Gruner, G. Microwave Shielding of Transparent and Conducting Single-Walled Carbon Nanotube Films. *Appl. Phys. Lett.* **2007**, *90*, 183119.
8. Son, K.-A. Nanostructure-Based Transparent Conductive Coating for RFI Shielding. Poster presented at the *NanoTechnology for Defense Conference*, Sumerlin, NV, 6–9 August 2012.
9. Adams, E. P. The Hall and Corbino Effects. *Proc. Am. Phil. Soc.* **1915**, *54*, 47–51.
10. Wu, Z. C.; Chen, Z. H.; Du, X.; Logan, J. M.; Sippel, J.; Nikolou, M.; Kamaras, K.; Reynolds, J. R.; Tanner, D. B.; Hebard, A. F.; Rinzler, A. G. Transparent, Conductive Carbon Nanotube Films. *Science* **2004**, *305*, 1273–1276.
11. MicroChem Corp., “LOR and PMGI Resists,” datasheet, Rev. A. Available: http://microchem.com/Prod-PMGI_LOR.htm (accessed 13 November 2012).
12. Collin, R. E. *Foundations for Microwave Engineering*; 2nd Ed., Wiley and Sons: Hoboken, NJ, 2001; pp 115–117.
13. Cheng, D. K. *Field and Wave Electromagnetics*; 2nd Ed., Addison-Wesley, Reading, PA, 1992; pp 440, 451, 466.

14. Kittel, C. Introduction to Solid State Physics, 7th Ed., Wiley and Sons: Hoboken, NJ, 1996; pp 273–274.
15. Low Level Measurements Handbook, 6th Ed., Keithley Instruments, Inc., Cleveland, OH, 2004; pp 2–42, 3–18, 4–51.
16. van der Pauw, L. J. A method of Measuring Specific Resistivity and Hall Effect of Discs of Arbitrary Shape. *Philips Res. Repts.* **1958**, *13*, 11.
17. Skin Depth–Microwave Encyclopedia–Microwaves101.com, November, 2010. [Online]. Available: <http://www.microwaves101.com/encyclopedia/skindepth.cfm> (accessed 14 November 2012).
18. Gordon, R. Criteria for Choosing Transparent Conductors. *MRS Bull.* **2000**, *25*, 52–57.
19. Electrical resistivity and conductivity–Wikipedia, the Free Encyclopedia, November 2012 [Online]. Available: http://en.wikipedia.org/wiki/Electrical_resistivity_and_conductivity#cite_note-serway-8 (accessed 14 November 2012).
20. Collins, P. G.; and Avouris, P. H. Nanotubes for Electronics. *Sci. Am.* **2000**, 283, 38.
21. Komatsu, N.; Wang, F. A. Comprehensive Review on Separation Methods and Techniques for Single-Walled Carbon Nanotubes. *Materials* **2010**, *3*, 3818-3844.
22. Duclaux, L. Review of the Doping of Carbon Nanotubes (Multiwalled and Single-Walled). *Carbon* **2002**, *40*, 1751.

List of Symbols, Abbreviations, and Acronyms

ARL	U.S. Army Research Laboratory
CNT	Carbon Nanotube
DUT	Device Under Test
EM	Electro-Magnetic
FoM	Figure-of-Merit
FTO	Fluorine-doped Tin Oxide
GND	ground
GRD	guard
ICPs	Intrinsically Conducting Polymers
ITO	Indium Tin Oxide
MUT	Material Under Test
PMGI	Poly(methyl glutarimide)
PGMEA	Propylene Glycol Monomethyl Ether Acetate
SEM	Scanning Electron Microscope
SIG	signal
SOL	Short-Open-Load
TCFs	Transparent Conducting Films
TCOs	Transparent Conducting Oxides
TEM	Transverse Electro-Magnetic
ZnO:F	fluorine-doped zinc oxide

NO. OF
COPIES ORGANIZATION

1 DEFENSE TECHNICAL
(PDF) INFORMATION CTR
only) DTIC OCA
8725 JOHN J KINGMAN RD
STE 0944
FORT BELVOIR VA 22060-6218

1 DIRECTOR
(PDF) US ARMY RESEARCH LAB
IMAL HRA
2800 POWDER MILL RD
ADELPHI MD 20783-1197

1 DIRECTOR
(PDF) US ARMY RESEARCH LAB
RDRL CIO LL
2800 POWDER MILL RD
ADELPHI MD 20783-1197

ABERDEEN PROVING GROUND

3 DIR USARL
(PDFs) RDRL WMM
J ZABINSKI
RDRL WMM E
R TOONEN (2 CPS)

INTENTIONALLY LEFT BLANK.